J Mater Sci (2007) 42:1782–1796
DOI 10.1007/s10853-006-0954-2

Principles of superplasticity in ultrafine-grained materials

Megumi Kawasaki · Terence G. Langdon

Received: 14 June 2006 / Accepted: 5 September 2006 / Published online: 13 February 2007

Abstract Ultrafine-grained materials are attractive for achieving superplastic elongations provided the grains are reasonably stable at elevated temperatures. Since the strain rate in superplasticity varies inversely with the grain size raised to a power of two, a reduction in grain size to the submicrometer level leads to the occurrence of superplastic flow within the region of high strain rate superplasticity at strain rates $>10^{-2}$ s^{-1}. This paper tabulates and examines the various reports of superplasticity in ultrafine-grained materials. It is shown that these materials exhibit many characteristics similar to conventional superplastic alloys including strain rates that are consistent with the standard model for superplastic flow and the development of internal cavitation during the flow process.

Introduction

Superplasticity refers to the ability of a polycrystalline material to pull out uniformly to a very high elongation in tension without the development of any incipient necking. Although there is no precise tensile elongation formally defining the advent of superplastic flow, it is generally considered that elongations to failure at and above ~500% are indicative of superplastic deformation. For many materials, the tensile elongations are often exceptionally high; for example, elongations of >7,000% were reported in a conventional two-phase Pb–62% Sn eutectic alloy [1]. When a metal is capable of deforming uniformly to very high strains, there is a potential for using the material to fabricate complex parts through simple superplastic forming operations. Commercial superplastic forming is currently in use for the manufacturing of parts for a range of industries including in aerospace, automotive and architectural applications [2].

Several recent reviews have covered the fundamental aspects of superplasticity [3–6]. It is now generally recognized that there are two basic requirements in order to achieve superplastic flow in a polycrystalline material [7]. First, the material must have a very small and stable grain size. Thus, the grain sizes used for materials in the superplastic forming industry are generally in the range of ~2–10 μm. Second, superplasticity is achieved only at relatively high temperatures because it is a diffusion-controlled process and therefore it is necessary to deform the material under conditions where diffusive flow is reasonably rapid. This means in practice that superplasticity is achieved at and above temperatures of the order of ~$0.5T_m$, where T_m is the absolute melting temperature of the material.

This paper describes the principles of attaining superplastic elongations in materials with exceptionally small grain sizes after processing using severe plastic deformation. To place this report in perspective, the following section provides a brief summary of superplasticity in conventional alloys and the subsequent

M. Kawasaki · T. G. Langdon (✉)
Departments of Aerospace & Mechanical Engineering and Materials Science, University of Southern California, Los Angeles, CA 90089-1453, USA
e-mail: langdon@usc.edu

T. G. Langdon
Materials Research Group, School of Engineering Sciences, University of Southampton, Southampton SO17 1BJ, UK

sections describe the characteristics of superplasticity in ultrafine-grained materials.

Principles of superplasticity in conventional alloys

Superplastic flow requires a grain size that is typically smaller than ~10 μm and therefore it is especially favored in two-phase materials where the presence of two separate phases leads to a significant inhibition in grain growth. An example is shown in Fig. 1 for a two-phase Zn–22% Al eutectoid alloy where the average spatial grain size, d, is 2.5 μm and the specimens were each pulled in tension to failure at absolute testing temperatures, T, from 423 to 503 K: the upper plot in Fig. 1 shows the measured elongations to failure, defined as $\Delta L/L_0\%$ where ΔL is the change in gauge length and L_0 is the initial gauge length, respectively, and the lower plot shows the flow stress, σ, as a function of the imposed strain rate, $\dot{\varepsilon}$ [8]. It is apparent from the lower plot that the datum points at each temperature divide into three well-defined regions having different values for the strain rate sensitivity, m, where m is defined as $(\partial \ln \sigma/\partial \ln \dot{\varepsilon})$. Thus, at low strain rates in region I there is a low strain rate

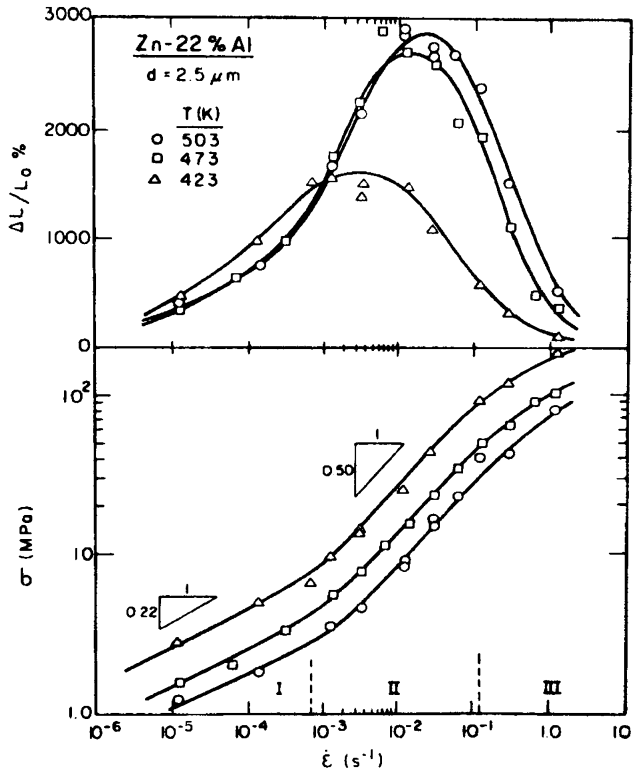

Fig. 1 Variation of the elongation to failure (upper) and the flow stress (lower) with the imposed strain rate for a Zn–22% Al eutectoid alloy tested over a range of temperatures [8]

sensitivity with $m \approx 0.22$, over a range of intermediate strain rates in region II, extending over approximately two orders of magnitude, there is a higher strain rate sensitivity with $m \approx 0.50$ and at the fastest strain rates in region III the strain rate sensitivity is again reduced and $m \approx 0.2$. The data in the upper plot show that superplastic ductilities are achieved only in region II where the tensile elongations extend up to >2000% whereas much smaller elongations are attained in regions I and III.

There are also two additional significant features in Fig. 1. First, it is apparent that high elongations are achieved most readily at the higher testing temperatures and there is a decrease in the overall ductility in region II when the testing temperature is reduced. Second, the peak or optimum elongations are displaced to faster strain rates when the temperature is increased. This latter effect is a natural consequence of the displacement to faster strain rates with increasing temperature of the stress–strain rate curves shown in the lower plot.

Detailed analysis has shown that superplastic flow occurs through the process of grain boundary sliding in which the individual grains of the polycrystalline matrix move over each other in response to the applied stress [9]. This flow process is defined formally as Rachinger sliding [10] and it occurs without any elongations of the individual grains. Thus, it varies in a very significant way from Lifshitz sliding [11] which accompanies conventional diffusion creep wherein the individual grains become elongated along the tensile axis [12]. A simple consideration of a polycrystalline array leads to the realization that the displacements of individual grains cannot occur in isolation and accordingly Rachinger sliding must be accommodated by some limited movement of dislocations within the adjacent grains. There are direct experimental observations confirming the presence of this intragranular flow in superplastic alloys. For example, the movement of intragranular dislocations was confirmed by measuring the densities of dislocations trapped in coherent twin boundaries in a superplastic copper alloy [13] and by directly measuring the intragranular strains occurring in a superplastic two-phase Pb–62% Sn eutectic alloy during flow in region II [14]. More recently, similar evidence was presented by demonstrating there are interactions between dislocations and particles within some of the grains of a superplastic Zn–22% Al alloy containing an array of dispersed particles [15, 16].

A simple model for the flow process in superplasticity is depicted schematically in Fig. 2. It is assumed that dislocations move along the grain boundary

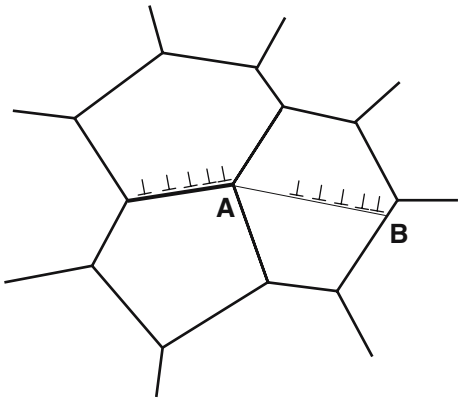

Fig. 2 Principles of a model for grain boundary sliding in superplasticity: dislocations move along the grain boundary and pile-up at the triple junction A, the stress concentration is removed by the nucleation of slip in the adjacent grain and these intragranular dislocations pile-up at B and climb into the grain boundary [17]

between two adjacent grains and pile-up at the triple junction labeled A. This generates a stress concentration so that slip is nucleated in the next grain and these dislocations move across the grain, pile-up at the opposing grain boundary at point B and are subsequently removed by climb into the boundary. It can be shown that this flow mechanism leads to a strain rate which is given by the expression:

$$\dot{\varepsilon} = A\left(\frac{DG\mathbf{b}}{kT}\right)\left(\frac{\mathbf{b}}{d}\right)^{p}\left(\frac{\sigma}{G}\right)^{n} \quad (1)$$

where the diffusion coefficient, D, is equal to D_{gb} for grain boundary diffusion, G is the shear modulus, **b** is the Burgers vector, k is Boltzmann's constant, the exponent of the inverse grain size, p, is ~2, the stress exponent, n (=1/m), is ~2 and A is a dimensionless constant having a value of ~10 [17].

An important characteristic of the mechanism illustrated in Fig. 2 is that the accommodating dislocations are able to glide through the blocking grain to impinge on the opposite grain boundary. It is apparent that this is possible only when the polycrystalline grain size is smaller than the equilibrium subgrain size, λ, thereby providing a direct explanation for experimental results showing that the superplastic region II occurs only when $d \leq \lambda$ [18]. Although Rachinger sliding in superplasticity follows Eq. 1 with $n \approx 2, p \approx 2$ and $D = D_{gb}$, it has been shown that a similar type of flow mechanism for Rachinger sliding in materials with larger grain sizes, where $d > \lambda$, leads to Eq. 1 with $D = D_{\ell}$, $n \approx 3$ and $p \approx 1$, where D_{ℓ} is the coefficient for lattice self-diffusion [17].

Principles of superplasticity in ultrafine-grained materials

Thermo-mechanical processing is used to produce alloys for industrial superplastic forming operations. Typically, the grain sizes of these materials are of the order of ~2–5 μm. However, it is now well established that processing through the introduction of severe plastic deformation provides the capability of producing grain sizes in the submicrometer or nanometer range [19]. For example, the process of equal-channel angular pressing (ECAP), where a sample is pressed through a die constrained within a channel bent through an abrupt angle, can be used to produce submicrometer grain sizes in a very wide range of metals [20]. This led to the proposal, first presented in 1996, that processes such as ECAP may be used to achieve superplastic behavior in metals at faster strain rates and/or at lower temperatures than in conventional superplastic alloys [21]. The reason for this proposal can be understood by considering the effect of reducing the grain size in Eq. 1.

Figure 3 illustrates the variation, on a logarithmic scale, of the strain rate, $\dot{\varepsilon}$, with the stress, σ, for superplastic alloys [22]. At high strain rates in region III there is a high slope, equivalent to a low value of m, in the region of dislocation creep where the material

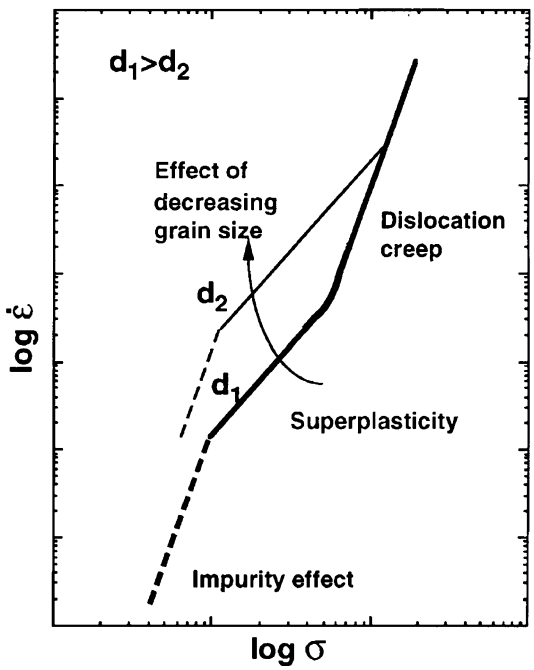

Fig. 3 Schematic illustration of the logarithmic variation of strain rate with stress for a conventional superplastic alloy with a grain size of d_1 and the displacement of the superplastic region to faster strain rates when the grain size is reduced to d_2 [22]

deforms by the glide and climb of dislocations within the grains: this region is equivalent to power-law creep occurring in materials with large grain sizes [23]. At intermediate strain rates, in the superplastic region II, the slope is given by $n \approx 2$ (equivalent to $m \approx 0.5$) and the material behaves superplastically. At even lower strain rates, in region I where n is again high, the behavior is controlled by impurity effects and the ductilities are no longer superplastic [24, 25]. The lower line in Fig. 3 depicts the situation for a material with a grain size of d_1. If the grain size is reduced to d_2 ($<d_1$), the behavior is unaffected in region III because $p = 0$ but the behavior in regions I and II is displaced upwards to faster strain rates because both regions have values of $p \approx 2$ in Eq. 1.

The displacement to faster rates in Fig. 3 is matched by a displacement in the peak ductilities to faster rates as shown schematically in Fig. 4 for d_1 and d_2 [22]. It is instructive to note that high strain rate superplasticity is defined formally as superplasticity occurring at strain rates at and above 10^{-2} s^{-1} [26] so that processing by ECAP and other similar techniques should provide an opportunity for achieving high strain rate superplasticity in a range of materials. Furthermore, as illustrated in Fig. 4, it is reasonable to anticipate the magnitudes of the peak elongations will be higher at the faster strain rates because less time is then available for the growth of any internal cavities.

The first demonstration of the occurrence of high strain rate superplasticity in an ultrafine-grained material occurred in 1997 when very high elongations were reported for an Al–5.5% Mg–2.2% Li–0.12% Zr alloy and an Al–6% Cu–0.4% Zr alloy [27]: the latter is a commercial alloy known as Supral 100 which is widely used in the superplastic forming industry. An example of this result is shown in Fig. 5 for the Al–Mg–Li–Zr alloy where the upper specimen is untested and the

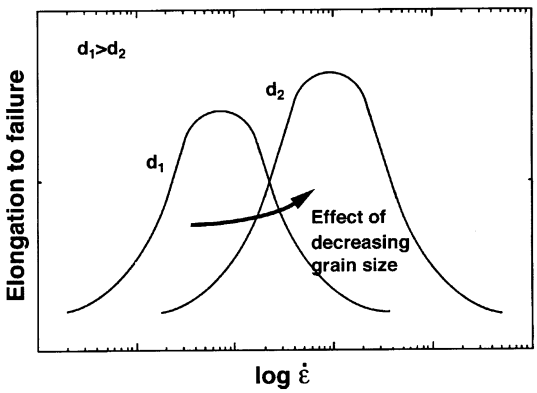

Fig. 4 Variation of the elongation to failure with strain rate when the grain size is reduced from d_1 to d_2 [22]

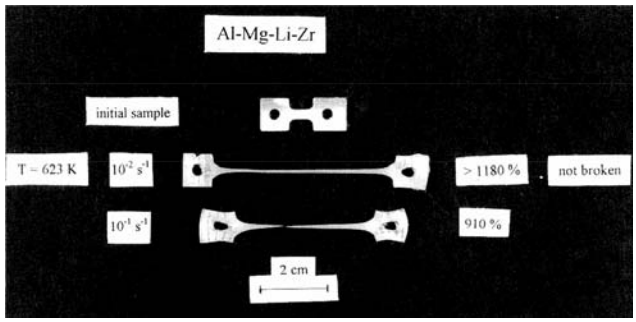

Fig. 5 The first example of high strain rate superplasticity reported in the literature for an ultrafine-grained Al–Mg–Li–Zr alloy in 1997 [27]

other two specimens were pulled in tension at 623 K after processing by ECAP through eight passes at 673 K and an additional four passes at 473 K: it can be shown from first principles that these pressing conditions, conducted with an ECAP die having an internal angle of 90°, lead to an imposed strain of ~12 [28]. In Fig. 5 the upper specimen was pulled to an elongation of 1,180% without failure at a strain rate of 10^{-2} s^{-1} and the lower specimen was pulled to failure at an elongation of 910% at a strain rate of 10^{-1} s^{-1}.

The results in Fig. 5 provide a very clear demonstration of the potential for achieving high strain rate superplasticity after processing alloys by ECAP. Since superplastic forming operations with conventional alloys generally take ~20–30 min for the fabrication of each separate component [29], it follows that processing by ECAP provides the opportunity of decreasing the grain size by close to one order of magnitude and, since $p \approx 2$ in Eq. 1, thereby increasing the optimum strain rate for superplasticity by approximately two orders of magnitude and reducing the forming time for each component to <60 s. Thus, the introduction of processing through severe plastic deformation leads to much faster forming operations and provides an opportunity for extending the superplastic forming industry into the production of high-volume components in the consumer product industries. Other potential applications of this approach include the production of medical implants, biomedical devices and parts for high-performance bicycles [30].

Characteristics of superplasticity in ultrafine-grained materials

Influence of the processing conditions

The occurrence of grain boundary sliding requires the presence of grain boundaries having high angles of

misorientation. This means in practice that the nature of the superplastic behavior is dictated by the processing conditions used to produce the ultrafine grain sizes. An example of this effect is shown in Fig. 6 for an Al–Mg–Li–Zr alloy where the samples in (a) were processed by ECAP through four passes at 673 K to a total strain of ~4 and the samples in (b) were processed through eight passes at 673 K and an additional four passes at 473 K to a total strain of ~12 [31]: both sets of specimens were processed in a die with an internal angle of 90° using processing route B_C where the samples are rotated by 90° in the same sense between each separate pass [32]. The solid datum points in Fig. 6 are for the unpressed alloy where it is apparent that the ductilities are consistently very low. The open points are for the alloy after pressing where the elongations to failure depend critically upon both the processing and the testing conditions. Thus, high strain rate superplasticity is achieved in both conditions but the exceptionally high elongations are displaced to faster strain rates in Fig. 6b when the material is processed through a larger number of passes. This result is consistent with experimental data for pure aluminum showing that the fraction of high-angle boundaries increases with increasing numbers of passes through the ECAP die [33].

The flow process in the superplasticity of ultrafine-grained materials

The relationship presented earlier in Eq. 1 was developed for conventional superplastic alloys where the grains sizes are typically ~2–5 μm. It is important, therefore, to determine whether the same approach applies equally to the superplastic flow observed in ultrafine-grained materials [34].

Figure 7 gives an example of superplastic results reported for an Al–3% Mg–0.2% Sc alloy pressed through eight passes using route B_C, where the upper plot shows the variation of the elongation to failure with the imposed strain rate at a testing temperature of 673 K and the lower plot shows the measured values of the flow stresses for each specimen [35]. Thus, this material exhibits exceptionally high ductility within the region of high strain rate superplasticity with elongations up to >2,000%. Superimposed on the lower plot is a broken line delineating the predictions from the relationship for superplastic flow given in Eq. 1 where $D_{gb} = 1.86 \times 10^{-4}\exp(-84{,}000/RT)$ m^2 s^{-1} where R is the gas constant [36], $G = \{(3.022 \times 10^4) - 16T\}$ MPa [36], $\mathbf{b} = 2.86 \times 10^{-10}$ m for pure Al, $p = 2$, $n = 2$, $A = 10$ and with the reported linear intercept grain size of $\bar{L} \approx 0.2\,\mu$m converted to a spatial grain size of $d = 1.74\bar{L} = 0.35\,\mu$m. It is apparent that the predicted line is in good agreement with the experimental data to within a factor of <3 on the stress axis within the region of optimum superplasticity. Thus, it is concluded that materials processed by severe plastic deformation exhibit a flow mechanism in the superplastic region which is identical to the flow behavior in conventional superplastic alloys where the grain sizes are larger by approximately one order of magnitude.

The occurrence of cavitation during superplastic flow in ultrafine-grained materials

It was demonstrated in a very early report that superplastic materials often contain significant levels of cavitation [37] and subsequently there have been numerous investigations of the role and development of internal cavitation in conventional superplastic alloys [4]. It is important, therefore, to evaluate the

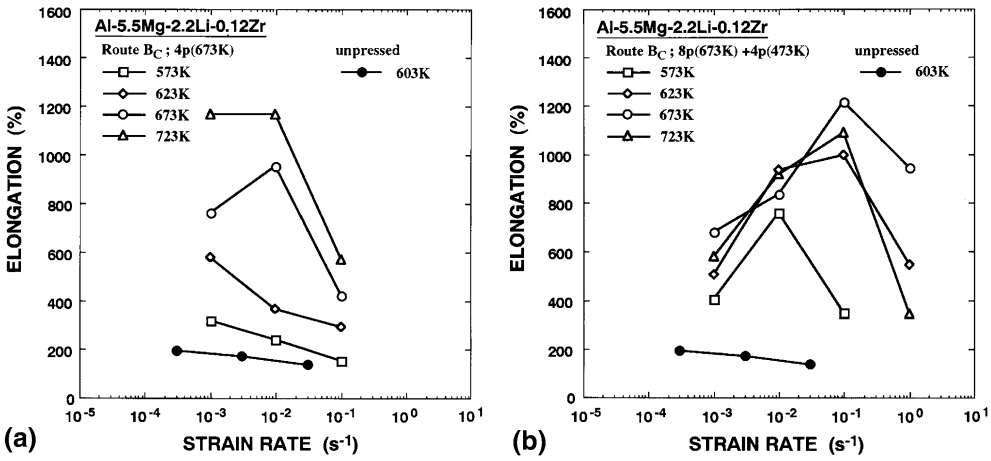

Fig. 6 Experimental results for an Al–Mg–Li–Zr alloy showing the displacement in the peak superplastic elongations to faster strain rates when ECAP processing is continued to higher strains: the solid points are for the unpressed material [31]

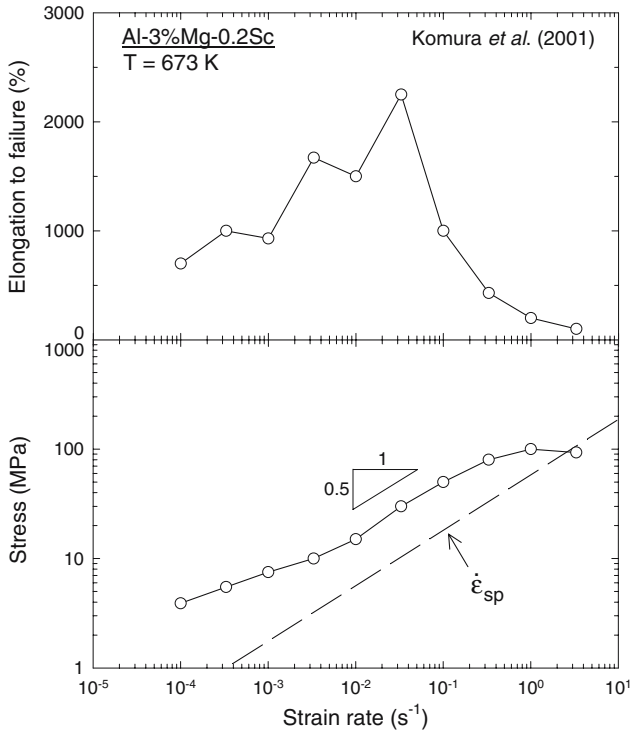

Fig. 7 Variation of the elongation to failure (upper) and the flow stress (lower) with the imposed strain rate for an Al–3% Mg–0.2% Sc alloy [35]: the broken line labeled $\dot{\varepsilon}_{sp}$ shows the predicted behavior using the model for grain boundary sliding in conventional superplastic alloys [17]

role of cavitation in superplastic materials processed by ECAP.

Experiments were conducted on a spray-cast Al-7034 alloy containing, in wt.%, Al–11.5% Zn–2.5% Mg–0.9% Cu–0.2% Zr and typical results are shown in Fig. 8 [38]. The results given in Fig. 8a are for the unpressed as-received alloy where the average grain size was ~2.1 μm whereas the results in Fig. 8b are for the alloy processed by ECAP at 473 K through either six passes (open points) or eight passes (solid points) to give a grain size of ~0.3 μm. It is apparent that excellent superplastic properties are achieved after ECAP and, as also documented earlier in Fig. 6, the peak elongation is displaced to a faster strain rate when the number of passes is increased.

Samples were examined for the presence of internal cavitation after pulling to failure and typical results are shown in Fig. 9 where the upper row relates to the as-received unpressed condition and the lower row shows specimens processed by ECAP for six passes at 473 K: the three separate photomicrographs in each row were taken at the same magnification and they correspond to the fracture tips at strain rates of 10^{-3}, 10^{-2} and 10^{-1} s^{-1}, respectively, with the tensile axis lying vertically [39]. Several features are apparent from inspection of Fig. 9. First, although the cavity densities are non-uniform and increase in the immediate vicinity of the fracture tips, nevertheless there appears to be a higher area fraction of cavities in the samples processed by ECAP. Second, the highly superplastic specimen shown in the center of the lower row, where the elongation to failure was 1,085%, exhibits no visible necking and failure occurs abruptly as a consequence of cavity inter-linkage. Detailed measurements were taken to evaluate the size and shape of these internal cavities and this led to the conclusion that, as in conventional superplastic alloys, there is a transition from the superplastic diffusion growth of cavities at the smaller cavity sizes [40] to plasticity-controlled growth at the larger sizes [41].

Discussion

A comparison of superplastic behavior in different ultrafine-grained materials

Although the first report of superplastic flow in alloys processed by ECAP was presented only in 1997 [27], there have been many subsequent reports of the occurrence of superplasticity in a very wide range of materials after processing by ECAP. To place these

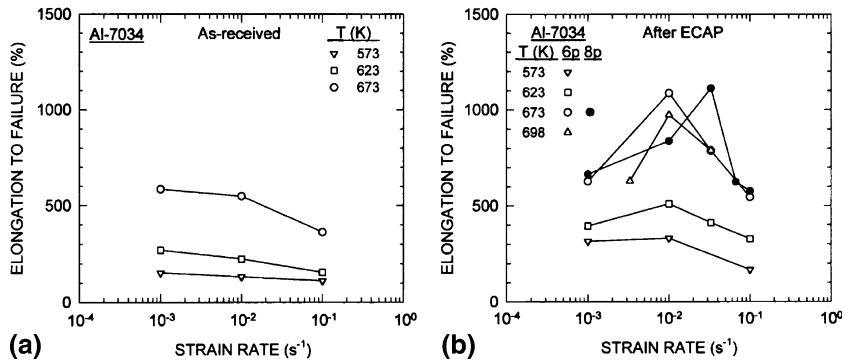

Fig. 8 Variation of elongation to failure with strain rate for an Al-7034 alloy in (**a**) the as-received and unpressed condition and (**b**) after processing by ECAP [38]

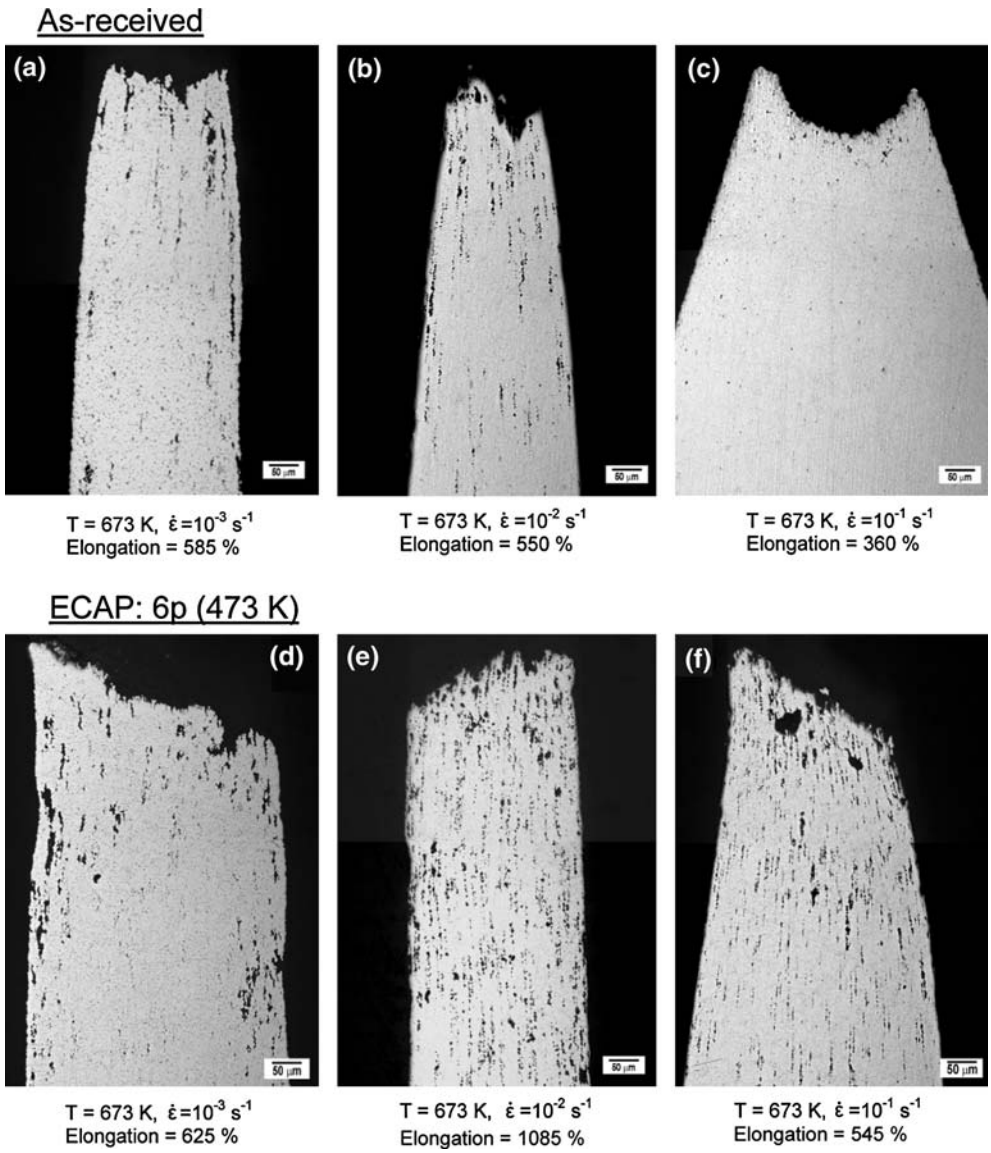

Fig. 9 Evidence for internal cavitation in the Al-7034 alloy after testing to failure: the upper row shows the as-received unpressed material and the lower row shows specimens processed by ECAP [39]

reports in perspective, the table in the Appendix presents a summary of the various reports of superplasticity published to date and, for convenience, the references from the table are numbered separately from the main text. In constructing the Appendix, superplastic elongations were defined specifically as elongations in tension of at least 500%. Thus, reports of lower elongations are not included.

The Appendix is divided into five parts. The first column gives the alloy or composition, with the matrix alloys arranged alphabetically and the various matrix alloys listed numerically for numbered designations and alphabetically for the others. The second main column headed ECAP summarizes the processing conditions in terms of the processing route, the number of passes, the channel angle between the two parts of the channel and the pressing temperature: processing route B_C was defined earlier, route A denotes pressing without rotation [32] and route B denotes a specimen taken through two passes with a rotation of 90°. The third main column gives the measured linear intercept grain size after ECAP. The fourth main column headed Superplasticity describes the testing conditions for the subsequent tensile tests, including the temperature and strain rate for the indicated maximum elongation. The fifth column gives the reference for each report. Following the Appendix, additional information is provided on the compositions of the alloys.

It is instructive to make a comparison between some of the results reported to date in terms of the alloy compositions. Figure 10 shows a plot of the optimum superplastic elongation taken from the Appendix for various alloys plotted against the measured grain size

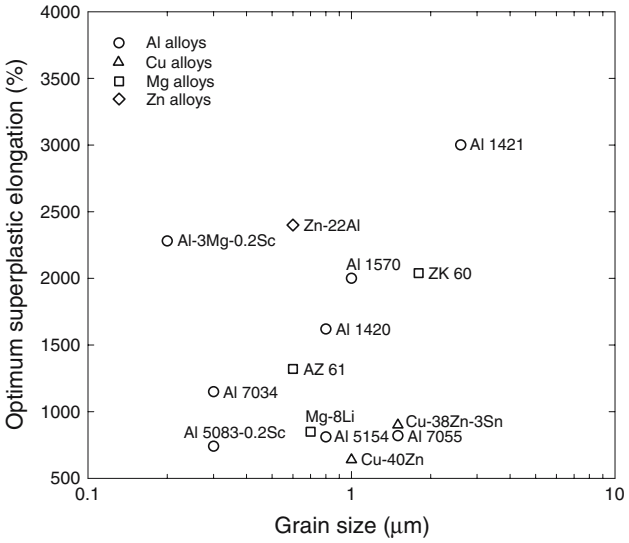

Fig. 10 Examples of the optimum superplastic elongations as a function of the grain size using experimental data from the Appendix

after ECAP: the plot is cut at 500% because this is taken as the lower limiting condition for true superplasticity and the plot contains various alloy designations but it is necessary to inspect the Appendix to find the relevant references. The plot in Fig. 10 shows the results are generally scattered and, because of the limited range of grain sizes, there is no clear evidence for increasing elongations at decreasing grain sizes. A similar plot is shown in Fig. 11 where the grain size is plotted against the strain rate for optimum superplasticity. When the data are plotted in this form, it is clear that a reduction in grain size favors the occurrence of superplasticity at faster strain rates. Thus, exceptionally fine grain sizes are a necessary objective for obtaining alloys capable of superplastic forming at very high strain rates.

An alternative approach is shown in Fig. 12 where two basic sets of fcc alloys, based on aluminum and copper, are compared with magnesium alloys and the Zn–22% Al eutectoid alloy: the data used for this plot were the optimum superplastic elongations and the associated testing strain rates. It is apparent that the Zn–22% Al alloy exhibits very high superplastic elongations at exceptionally rapid strain rates with elongations up to >2,000% at a strain rate of 1 s^{-1} [42], where this remarkable result is probably due to the thermal stability of the microstructure because of the presence of two separate phases. The data for the two sets of fcc alloys show results spanning the onset of high strain rate superplasticity at a strain rate of 10^{-2} s^{-1} whereas the magnesium-based alloys exhibit superplastic flow at strain rates which are generally relatively low although there is an isolated report of an elongation of 1,400% in a ZK60 alloy at an imposed strain rate of 3.0×10^{-2} s^{-1} [43].

A comparison of ECAP with other processing techniques

Two very useful diagrams were developed several years ago to delineate the ranges of strain rates and grain sizes associated with the occurrence of superplasticity in aluminum-based alloys when processed in a number of different ways [44]. It is instructive to use these same plots and to incorporate the results now available from processing by ECAP. These two plots are shown in Figs. 13 and 14 where, respectively, typical elongations to failure and the spatial grain sizes are plotted against the testing strain rate. In these plots, the solid circles and ovals denote areas

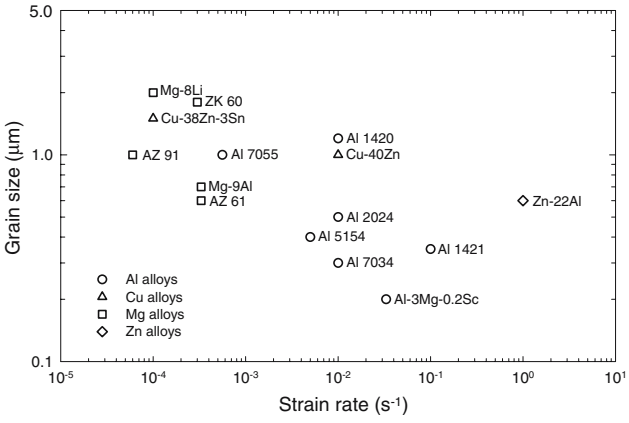

Fig. 11 Examples of the variation of grain size with strain rate under conditions of optimum superplastic ductility using experimental data from the Appendix

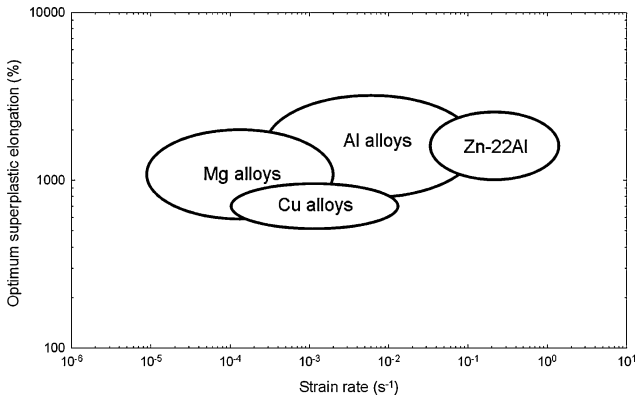

Fig. 12 The optimum superplastic elongations as a function of strain rate for various classes of alloys using the experimental data in the Appendix

associated with various aluminum alloys processed using a range of techniques from ingot metallurgy at the slow rates on the left to powder metallurgy (PM) at strain rates of ~10^{-2} to ~1 s^{-1} in the center and to other processing techniques such as physical vapor deposition, mechanical alloying and consolidation from amorphous or nanocrystalline powders at even faster strain rates. Both plots indicate the defined range associated with high strain rate superplasticity and, at the top of each diagram, the range currently associated with commercial superplastic forming.

Superimposed in Fig. 13 and 14, and delineated by the broken lines, are the regions associated with superplasticity in aluminum-based alloys processed by ECAP. These areas are constructed based on a detailed appraisal of the information in the Appendix and they represent a best estimate of the conditions associated with optimum superplasticity for these ultrafine-grained alloys. In inserting the data onto Fig. 14, the mean linear intercept grain sizes reported in ECAP were converted to the spatial grain sizes using the relationship given earlier in ''The flow process in the superplasticity of ultrafine-grained materials'' section.

It is readily apparent that the data for ECAP processing fit appropriately into the two diagrams originally constructed for more conventional superplastic alloys. Specifically, it is apparent in Fig. 13 that the use of ECAP processing extends the data for ingot metallurgy materials to faster strain rates and provides a useful overlap with the field for materials processed using powder metallurgy techniques. In this respect, ECAP processing has an advantage because it can be conducted on ingot metal stock without introducing

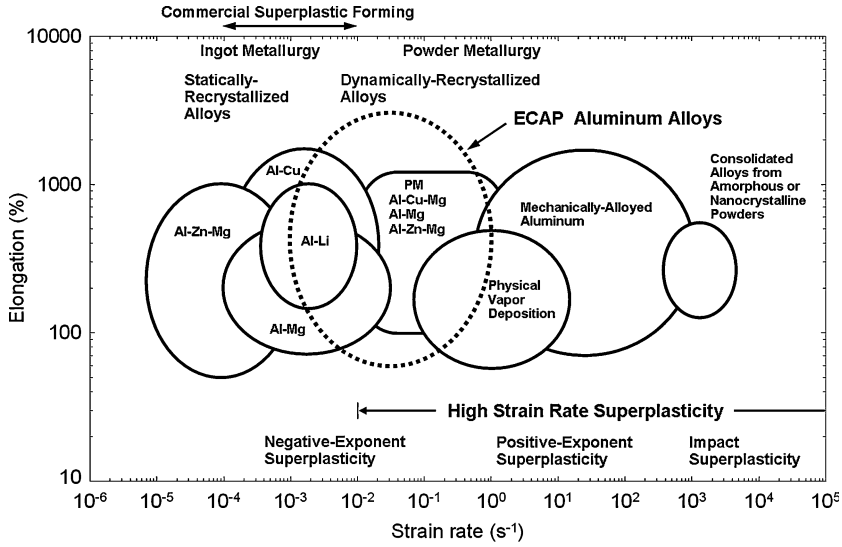

Fig. 13 The regime of aluminum alloys processed by ECAP superimposed on the standard plot of elongation versus strain rate for a range of processing techniques [44]

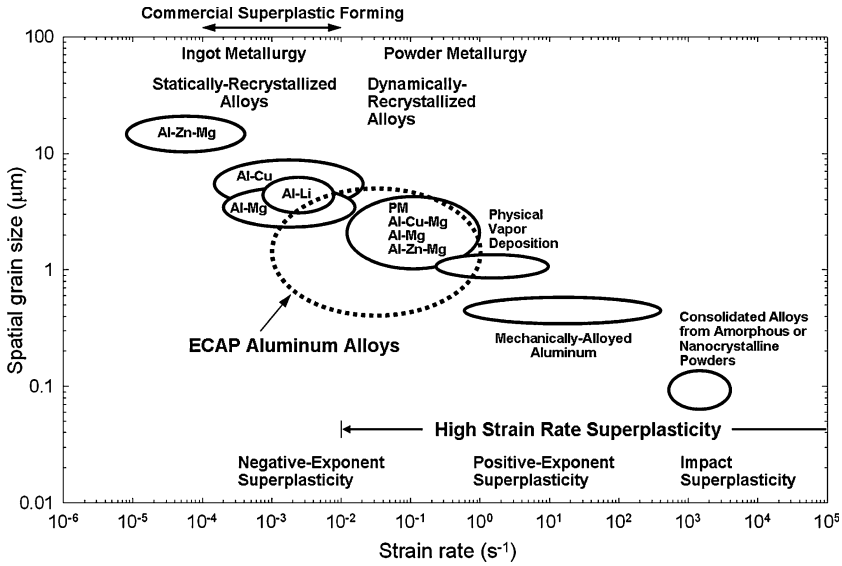

Fig. 14 The regime of aluminum alloys processed by ECAP superimposed on the standard plot of grain size versus strain rate for a range of processing techniques [44]: the mean linear intercept grain sizes reported in ECAP were converted to the spatial grain sizes for this representation

either contamination or cavitation into the end product. In Fig. 14 the materials processed by ECAP again fit appropriately in the overlap region between the ingot metallurgy and powder metallurgy materials. This plot also provides a direct correlation with the data for the various alloys presented earlier in Fig. 11 although it is important to note that Fig. 11 incorporates the standard mean linear intercept grain size whereas in Fig. 14 the grain sizes relate to the spatial values. Despite this minor difference, it is readily concluded from Figs 13 and 14 that processing by ECAP represents an important tool for extending the viability of aluminum-based alloys without using either powder metallurgy techniques or more exotic processing routes involving deposition, consolidation or mechanical alloying.

Summary and conclusions

1. Processing by severe plastic deformation, as in equal-channel angular pressing, produces ultrafine grain sizes typically in the submicrometer range. If these small grains have reasonable thermal stability, the materials will exhibit excellent superplastic ductilities at elevated temperatures. Furthermore, the reduction in grain size to the submicrometer level leads to the occurrence of superplasticity at very high strain rates by comparison with conventional superplastic materials.
2. There have been numerous reports of superplasticity in ultrafine-grained materials since the first report appeared in 1997. These reports are tabulated and examined. It is demonstrated that there are several similarities to conventional superplastic alloys including the occurrence of superplastic flow at strain rates which are consistent with a model developed for conventional superplasticity and the development of internal cavitation during the flow process.
3. It is shown that the processing of cast metals by ECAP provides the opportunity of attaining superplasticity at strain rates which are comparable to those normally associated with powder metallurgy products.

Acknowledgement This work was supported by the U.S. Army Research Office under Grant No. W911NF-05-1-0046.

References

1. Ma Y, Langdon TG (1994) Metall Mater Trans 25A:2309
2. Barnes AJ (2001) Mater Sci Forum 357–359:3
3. Chokshi AH, Mukherjee AK, Langdon TG (1993) Mater Sci Eng R10:237
4. Jiang XG, Earthman J, Mohamed FA (1994) J Mater Sci 29:5499
5. Nieh TG, Wadsworth J, Sherby OD (1997) Superplasticity in metals and ceramics. Cambridge University Press, Cambridge, U.K
6. Kaibyshev OA, Utyashev FZ (2005) Superplasticity: microstructural refinement and superplastic roll forming. Futurepast, Arlington, VA
7. Langdon TG (1982) Metall Trans 13A:689
8. Mohamed FA, Ahmed MMI, Langdon TG (1977) Metall Trans 8A:933
9. Langdon TG (1994) Mater Sci Eng A 174:225
10. Rachinger WA (1952–53) J Inst Metals 81:33
11. Lifshitz IM (1963) Soviet Phys JETP 17:909
12. Langdon TG (2006) J Mater Sci 41:597
13. Falk LKL, Howell PR, Dunlop GL, Langdon TG (1986) Acta Metall 34:1203
14. Valiev RZ, Langdon TG (1993) Acta Metall Mater 41:949
15. Xun Y, Mohamed FA (2003) Phil Mag 83:2247
16. Xun Y, Mohamed FA (2004) Acta Mater 52:4401
17. Langdon TG (1994) Acta Metall Mater 42:2437
18. Mohamed FA, Langdon TG (1976) Scr Mater 10:759
19. Valiev RZ, Islamgaliev RK, Alexandrov IV (2000) Prog Mater Sci 45:103
20. Valiev RZ, Langdon TG (2006) Prog Mater Sci 51:881
21. Ma Y, Furukawa M, Horita Z, Nemoto M, Valiev RZ, Langdon TG (1996) Mater Trans JIM 37:336
22. Xu C, Furukawa M, Horita Z, Langdon TG (2003) Adv Eng Mater 5:359
23. Kassner ME, Pérez-Prado M-T (2000) Prog Mater Sci 45:1
24. Mohamed FA (1983) J Mater Sci 18:582
25. Mohamed FA (1988) J Mater Sci Lett 7:215
26. Higashi K, Mabuchi M, Langdon TG (1996) ISIJ Intl 36:1423
27. Valiev RZ, Salimonenko DA, Tsenev NK, Berbon PB, Langdon TG (1997) Scr Mater 37:1945
28. Iwahashi Y, Wang J, Horita Z, Nemoto M, Langdon TG (1996) Scr Mater 35:143
29. Barnes AJ (1999) Mater Sci Forum 304–306:785
30. Zhu YT, Lowe TC, Langdon TG (2004) Scr Mater 51:825
31. Lee S, Berbon PB, Furukawa M, Horita Z, Nemoto M, Tsenev NK, Valiev RZ, Langdon TG (1999) Mater Sci Eng A 272:63
32. Furukawa M, Iwahashi Y, Horita Z, Nemoto M, Langdon TG (1998) Mater Sci Eng A 257:328
33. Terhune SD, Swisher DL, Oh-ishi K, Horita Z, Langdon TG, McNelley TR (2002) Metall Mater Trans 33A:2173
34. Balasubramanian N, Langdon TG (2005) Mater Sci Eng A 410–411:476
35. Komura S, Horita Z, Furukawa M, Nemoto M, Langdon TG (2001) Metall Mater Trans 32A:707
36. Mohamed FA, Langdon TG (1974) Metall Trans 5:2339
37. Ishikawa H, Bhat DG, Mohamed FA, Langdon TG (1977) Metall Trans 8A:523
38. Xu C, Furukawa M, Horita Z, Langdon TG (2003) Acta Mater 51:6139
39. Kawasaki M, Xu C, Langdon TG (2005) Acta Mater 53:5353
40. Chokshi AH, Langdon TG (1987) Acta Metall 35:1089
41. Hancock JW (1976) Metal Sci 10:319
42. Lee S-M, Langdon TG (2001) Mater Sci Forum 357–359:321
43. Lapovok R, Cottam R, Thomson PF, Estrin Y (2005) J Mater Res 20:1375
44. Higashi K (1994) Mater Sci Forum 170–172:131

Appendix

Appendix Reports of superplasticity in ultrafine-grained materials

Alloy or composition (wt.%)	ECAP				Grain size (μm)	Superplasticity			Reference
	Processing route	Number of passes	Channel angle	Temperature (K)		Testing temperature (K)	Strain rate (s^{-1})	Maximum elongation	
Al 1420[1] Al 2004[2]	B_C	12	90°	673 (8p) + 473 (4p)	1.2 0.5	623 573	1.0×10^{-2} 1.0×10^{-2}	1180% 970%	Valiev et al. (1997) [1]
Al 1420–0.2 Sc	B_C	4 12	90°	673 673 (8p) + 473 (4p)	1.2 1.2	603 623	3.3×10^{-3} 1.0×10^{-2}	550% >1180%	Berbon et al. (1998) [2]
Al 1420	B_C	4	90°	673	1.2	603	3.3×10^{-3}	550%	Furukawa et al. (1998) [3]
Al 1420	B_C	4 8 12	90°	673 673 673 (8p) + 473 (4p)	1.2 1.3 0.8	723 673 673	1.0×10^{-2} 1.0×10^{-2} 1.0×10^{-1}	1170% 1250% 1210%	Lee et al. (1999) [4]
Al 1420 Al 1421[3]	B_C	10	90°	643	1.1	673	1.0×10^{-2}	820%	Kolobov et al. (2004) [5]
Al 1420 Al 1421	B_C	10	90°	643 643	0.7–0.9 0.3–0.4	673 673	1.0×10^{-2} 1.0×10^{-1}	1620% >1500%	Islamgaliev et al. (2006) [6]
Al 1421	B_C	12	90°	643	0.3–0.4	673	1.0×10^{-1}	1500%	Islamgaliev et al. (2003) [7]
Al 1421	B_C	12 16 16	90°	513 598 673	0.6 0.8 2.6	673 673 723	1.4×10^{-2}	740% 2100% 3000%	Kaibyshev et al. (2005) [8]
Al 1421	B_C	12	90°	643	1	700	1.0×10^{-2}	840%	Naidenkin et al. (2006) [9]
Al 1421 Al 1460[4]	B_C	–	90°	623	0.5	623	2.0×10^{-2}	1220% 670%	Shammazov et al. (2000) [10]
Al 1570[5]	B_C	16	90°	598	1	723	5.6×10^{-2}	2000%	Musin et al. (2004) [11], (2004) [12]
Al 2024[6]	B_C	8	90°	373	0.5	673	1.0×10^{-2}	500%	Lee et al. (2003) [13]
Al 5083–0.2 Sc[7]	B_C	4	90°	473	0.3	773	1.0×10^{-2}	740%	Park et al. (2003) [14], Shin et al. (2004) [15]
Al 5083–0.2 Sc	B_C	4	90°	473	0.2–0.4	773	1.0×10^{-2}	740%	Park et al. (2005) [16]

Appendix continued

Alloy or composition (wt.%)	ECAP				Grain size (μm)	Superplasticity			Reference
	Processing route	Number of passes	Channel angle	Temperature (K)		Testing temperature (K)	Strain rate (s^{-1})	Maximum elongation	
Al 5154[8, a] Al 5154	B_C	4 8	90°	473	0.2–0.4	723	5.0×10^{-3} 1.0×10^{-2}	810% 590%	Park et al. (2004) [17]
Al 5154[a]	B_C	4	90°	473	1	723	5.0×10^{-3}	810%	Park et al. (2006) [18]
Al 7034[9]	B_C	6	90°	473	0.3	623	1.0×10^{-2}	510%	Xu et al. (2003) [19]
Al 7034	B_C	6 8	90°	473	0.3	673	1.0×10^{-2} 3.3×10^{-2}	1090% 1110%	Xu et al. (2003) [20], (2005) [21]
Al 7034	B_C	4	90°	473	0.3	673	1.0×10^{-2}	870%	Xu and Langdon (2005) [22]
Al 7034	B_C	6	90°	473	0.3	673	1.0×10^{-2}	1090%	Kawasaki et al. (2005) [23]
Al 7055[10]	A	4	90°	573	1	698	5.6×10^{-4}	750%	Kaibyshev et al. (2003) [24]
Al 7055[b]	A	10	90°	523	1.4	723	5.6×10^{-3}	820%	Nikulin et al. (2005) [25]
Al–3 Mg–0.2 Sc	B_C	8	90°	RT	0.2	673	3.3×10^{-2}	1030%	Komura et al. (1998) [26]
Al–3 Mg–0.2 Sc	B_C	8 12	90°	RT	0.2 0.2	673	3.3×10^{-2} 3.3×10^{-2}	1030% 1560%	Berbon et al. (1999) [27]
Al–3 Mg–0.2 Sc	B_C	8	90°	RT	0.2	673	3.3×10^{-2}	2280%	Horita et al. (2000) [28]
Al–3 Mg–0.2 Sc	B_C	8	90°	RT	0.2	673	3.3×10^{-2}	2280%	Komura et al. (2000) [29]
Al–3 Mg–0.2 Sc[c]	B_C	8	90°	RT	0.2	673	3.3×10^{-2}	1860%	Akamatsu et al. (2001) [30]
Al–1 Mg–0.2 Sc Al–3 Mg–0.2 Sc	B_C	8	90°	RT	0.36 0.2	673	1.0×10^{-3} 3.3×10^{-2}	580% 2280%	Furukawa et al. (2001) [31]
Al–3 Mg–0.2 Sc	B_C	8 12	90°	RT	0.2 0.2	673	3.3×10^{-2}	2280% 1820%	Komura et al. (2001) [32]
Al–3 Mg–0.2 Sc	B_C	8	90°	RT	0.2	723	3.3×10^{-3}	2580%	Komura et al. (2001) [33]
Al–3 Mg–0.2 Sc Al–3 Mg–0.2 Sc–0.12 Zr	B_C	8 6	90°	RT	0.2 0.3	573 773	1.0×10^{-2} 1.0×10^{-2}	1280% 1680%	Lee et al. (2002) [34]
Al–3 Mg–0.2 Sc	B_C	8	90°	RT	0.2	523	3.3×10^{-4}	640%	Ota et al. (2002) [35]

Appendix continued

Alloy or composition (wt.%)	ECAP				Grain size (μm)	Superplasticity			Reference
	Processing route	Number of passes	Channel angle	Temperature (K)		Testing temperature (K)	Strain rate (s^{-1})	Maximum elongation	
Al–3 Mg–0.2 Sc	B_C	8	90°	RT	0.2	673	3.3×10^{-2}	550%[d] 580%[e] 450%[f]	Sakai et al. (2003) [36]
Al–0.22 Sc–0.15 Zr	B_C	6	90°	448	1.5	673	1.0×10^{-2}	540%	Perevezentsev et al. (2002) [37]
Al–1.5 Mg–0.22 Sc–0.15 Zr		6			1.2	723	1.0×10^{-1}	1590%	
		8			1.2	723	1.0×10^{-2}	1400%	
Al–3 Mg–0.22 Sc–0.15 Zr		6			2	723	1.0×10^{-1}	2280%	
Al–4.5 Mg–0.22 Sc–0.15 Zr		6			1	723	3.3×10^{-2}	2250%	
Al–0.22 Sc–0.15 Zr	B_C	6	90°	448	1	673	1.0×10^{-2}	540%	Perevezentsev et al. (2002) [38]
Al–1.5 Mg–0.22 Sc–0.15 Zr		6			0.1	723	1.0×10^{-1}	1200%	
		8			0.1	723	1.0×10^{-2}	1400%	
Al–3 Mg–0.22 Sc–0.15 Zr		6			0.5	723	1.0×10^{-1}	680%	
Al–4.5 Mg–0.22 Sc–0.15 Zr		6			0.1	723	3.3×10^{-2}	2250%	
Cu–40 Zn	B_C	1	90°	673	1	673	1.0×10^{-2}	640%	Neishi et al. (2001) [39]
Cu–38 Zn–3 Sn	B	2	90°	673	1.5	573 673	1.0×10^{-3} 1.0×10^{-4}	675% 900%	Neishi et al. (2001) [40]
AZ 61[11]	B_C	6	90°	473 (2p) + 448 (4p)	<1	448	3.0×10^{-5}	1190%	Yoshida et al. (2004) [41]
AZ 61	B_C	4	90°	473	0.6	473	3.3×10^{-4}	1320%	Miyahara et al. (2006) [42]
AZ 91[12]	–	8	–	448	1	473	6.0×10^{-5}	661%	Mabuchi et al. (1997) [43–45]
AZ 91[g]	–	6	90°	448	0.5	473	7.0×10^{-5}	956%	Mabuchi et al. (1999) [46]
AZ 91 ZK 60[13]	B_C	6	90°	473~523 453~503	0.8 1	573 533	3.0×10^{-3} 6.5×10^{-4}	570% 960%	Chuvil'deev et al. (2004) [47, 48]
ZK 40[14]	–	3	–	–	<1	523	1.0×10^{-3}	612%	Lin et al. (2006) [49]

Appendix continued

Alloy or composition (wt.%)	ECAP				Grain size (μm)	Superplasticity			Reference
	Processing route	Number of passes	Channel angle	Temperature (K)		Testing temperature (K)	Strain rate (s^{-1})	Maximum elongation	
ZK 60	B_C	8	90°	433	1.4	473	1.0×10^{-5}	1083%	Watanabe et al. (2002, 2003) [50, 51]
ZK 60	B_C	6	90°	473	Bi-modal 1.8 ± 1.5 and 12.5±2.2	493	3.0×10^{-3} 3.0×10^{-4}	1400% 2040%	Lapovok et al. (2005) [52]
ZK 60	B_C	Roll (75%) + 6 6	90°	473	Bi-modal	493	3.0×10^{-4}	860% 2040%	Lapovok et al. (2005) [53]
ZK 60	B_C	6	90°	473	0.8	473	2.0×10^{-4}	1310%	Figueiredo and Langdon (2006) [54]
Mg–7.5 Al–0.2 Zr	B_C	2	90°	473	0.8	448	3.3×10^{-4}	760%	Miyahara et al. (2005) [55]
Mg–9 Al	B_C	2	90°	473	0.7	473	3.3×10^{-4}	840%	Matsubara et al. (2003) [56]
Mg–8 Li	B	2	110°	473	1–3	473	1.0×10^{-4}	970%	Furui et al. (2005) [57]
Mg–8 Li	B_C	2	135°	RT	2.5	473	1.0×10^{-4}	1610%	Furui et al. (2007) [58]
Mg–8 Li	B_C	2	135°	RT	1–3	473	1.5×10^{-4}	1780%	Furui et al. (2007) [59]
Zn–22 Al	B_C	8	90°	373	0.4–0.8	423 473	3.3×10^{-3} 3.3×10^{-2}	940% 1970%	Furukawa et al. (1998) [60]
Zn–22 Al	B_C	12	90°	373	0.6	533	1.0	>2380%	Lee and Langdon (2001) [61]

Alloy designations. [1]Al 1420: Al–5.5 Mg–2.2 Li–0.12 Zr; [2]Al 2004: Al–6 Cu–0.4 Zr; [3]Al 1421: Al–5 Mg–2.2 Li–0.12 Zr–0.2 Sc; [4]Al 1460: Al–2.65 Cu–2.2 Li–0.12 Zr; [5]Al 1570: Al–5.76 Mg–0.32 Sc–0.3 Mn–0.2 Si–0.1 Fe; [6]Al 2024: Al–4.4 Cu–1.5 Mg–0.6 Mn; [7]Al 5083-0.2 Sc: Al–4.2 Mg–0.6 Mn–0.1 Cr–0.2 Sc; [8]Al 5154: Al–3.22 Mg–0.13 Sc–0.07 Fe–0.04 Si–0.01 Zn–0.007 Ti–0.005 Cu–0.002 Mn; [9]Al 7034: Al–11.5 Zn–2.5 Mg–0.9 Cu–0.2 Zr; [10]Al 7055: Al–8.2 Zn–2.1 Mg–2.2 Cu–0.2 Zr–0.09 Mn–0.09 Fe–0.07 Si–0.04 Ni–0.02 Ti–0.08 Cr; [11]AZ 61: Mg–6 Al–1 Zn; [12]AZ 91: Mg–9 Al–1 Zn–0.2 Mn; [13]ZK 60: Mg–6 Zn–0.5 Zr; [14]ZK 40: Mg–3.73 Zn–0.64 Zr

[a] The Al 5154 was processed by ECAP and subsequent cold rolling (70% reduction)

[b] The Al 7055 was processed by ECAP and subsequent isothermal rolling (523 K)

[c] The Al–3 Mg–0.2 Sc was processed by ECAP and cold rolling

[d–f] For Al–3 Mg–0.2 Sc, gauge lengths of tensile specimens parallel to *X*, *Y* or *Z* directions, respectively

[g] The AZ 91 was processed by ECAP and annealed at 498 K for 12 h

Appendix references

1. Valiev RZ, Salimonenko DA, Tsenev NK, Berbon PB, Langdon TG (1997) Scr Mater 37:1945
2. Berbon PB, Furukawa M, Horita Z, Nemoto M, Tsenev NK, Valiev RZ, Langdon TG (1998) Phil Mag Lett 78:313
3. Furukawa M, Berbon PB, Horita Z, Nemoto M, Tsenev NK, Valiev RZ, Langdon TG (1998) Metall Mater Trans 29A:169
4. Lee S, Berbon PB, Furukawa M, Horita Z, Nemoto M, Tsenev NK, Valiev RZ, Langdon TG (1999) Mater Sci Eng A 272:63
5. Kolobov YuR, Dudarev EF, Langdon TG, Pochivalova GP, Naidenkin EV (2004) Russian Metall 2004(2):116
6. Islamgaliev RK, Yunusova NF, Valiev RZ (2006) Mater Sci Forum 503–504:585
7. Islamgaliev RK, Yunusova NF, Valiev RZ, Tsenev NK, Perevezentsev VN, Langdon TG (2003) Scr Mater 49:467
8. Kaibyshev R, Shipilova K, Musin F, Motohashi Y (2005) Mater Sci Tech 21:408
9. Naidenkin EV, Dudarev EF, Kolobov YuR, Bakach GP, Langdon TG (2006) Mater Sci Forum 503–504:983
10. Shammazov AM, Tsenev NK, Valiev RZ, Myshlyaev MM, Bikbulatov MM, Lebedich SP (2000) Phys Met Metall 89:314
11. Musin F, Kaibyshev R, Motohashi Y, Itoh G (2004) Metall Mater Trans 35A:2383
12. Musin F, Kaibyshev R, Motohashi Y, Itoh G (2004) Scr Mater 50:511
13. Lee S, Furukawa M, Horita Z, Langdon TG (2003) Mater Sci Eng A 342:294
14. Park K-T, Hwang D-Y, Lee Y-K, Kim Y-K, Shin DH (2003) Mater Sci Eng A 341:273
15. Shin DH, Hwang D-Y, Oh Y-J, Park K-T (2004) Metall Mater Trans 35A:825
16. Park K-T, Lee CS, Shin DH (2005) Mater Sci Forum 475–479:2937
17. Park K-T, Lee H-J, Lee CS, Nam WJ, Shin DH (2004) Scr Mater 51:479
18. Park K-T, Lee CS, Kim YS, Shin DH (2006) Mater Sci Forum 503–504:119
19. Xu C, Dixon W, Furukawa M, Horita Z, Langdon TG (2003) Mater Lett 57:3588
20. Xu C, Furukawa M, Horita Z, Langdon TG (2003) Acta Mater 51:6139
21. Xu C, Furukawa M, Horita Z, Langdon TG (2005) Acta Mater 53:749
22. Xu C, Langdon TG (2005) Mater Sci Eng A 410–411:398
23. Kawasaki M, Xu C, Langdon TG (2005) Acta Mater 53:5353
24. Kaibyshev R, Sakai T, Nikulin I, Musin F, Goloborodko A (2003) Mater Sci Tech 19:1491
25. Nikulin I, Kaibyshev R, Sakai T (2005) Mater Sci Eng A 407:62
26. Komura S, Berbon PB, Furukawa M, Horita Z, Nemoto M, Langdon TG (1998) Scr Mater 38:1851
27. Berbon PB, Komura S, Utsunomiya A, Horita Z, Furukawa M, Nemoto M, Langdon TG (1999) Mater Trans JIM 40:772
28. Horita Z, Furukawa M, Nemoto M, Barnes AJ, Langdon TG (2000) Acta Mater 48:3633
29. Komura S, Horita Z, Furukawa M, Nemoto M, Langdon TG (2000) J Mater Res 15:2571
30. Akamatsu H, Fujinami T, Horita Z, Langdon TG (2001) Scr Mater 44:759
31. Furukawa M, Utsunomiya A, Matsubara K, Horita Z, Langdon TG (2001) Acta Mater 49:3829
32. Komura S, Furukawa M, Horita Z, Nemoto M, Langdon TG (2001) Mater Sci Eng A 297:111
33. Komura S, Horita Z, Furukawa M, Nemoto M, Langdon TG (2001) Metall Mater Trans 32A:707
34. Lee S, Utsunomiya A, Akamatsu H, Neishi K, Furukawa M, Horita Z, Langdon TG (2002) Acta Mater 50:553
35. Ota S, Akamatsu H, Neishi K, Furukawa M, Horita Z, Langdon TG (2002) Mater Trans 43:2364
36. Sakai G, Horita Z, Langdon TG (2004) Mater Trans 45:3079
37. Perevezentsev VN, Chuvil'deev VN, Sysoev AN, Kopylov VI, Langdon TG (2002) Phys Met Metall. 94 (Suppl 1):S45
38. Perevezentsev VN, Chuvil'deev VN, Kopylov VI, Sysoev AN, Langdon TG (2002) Ann Chim Sci Mat 27:99
39. Neishi K, Horita Z, Langdon TG (2001) Scr Mater 45:965
40. Neishi K, Uchida T, Yamauchi A, Nakamura K, Horita Z, Langdon TG (2001) Mater Sci Eng A 307:23
41. Yoshida Y, Arai K, Itoh S, Kamado S, Kojima Y (2004) Mater Trans 45:2537
42. Miyahara Y, Horita Z, Langdon TG (2006) Mater Sci Eng A 420:240
43. Mabuchi M, Iwasaki H, Yanase K, Higashi K (1997) Scr Mater 36:681
44. Mabuchi M, Nakamura M, Ameyama K, Iwasaki H, Higashi K (1999) Mater Sci Forum 304–306:67
45. Mabuchi M, Iwasaki H, Higashi K (1997) Mater Sci Forum 243–245:547
46. Mabuchi M, Ameyama K, Iwasaki H, Higashi K (1999) Acta Mater 47:2047
47. Chuvil'deev VN, Nieh TG, Gryaznov MYu, Kopylov VI, Sysoev AN (2004) J Alloys Compd 378:253
48. Chuvil'deev VN, Nieh TG, Gryaznov MYu, Sysoev AN, Kopylov VI (2004) Scr Mater 50:861
49. Lin L, Wu W, Yang L, Chen L, Liu Z (2006) J Mater Sci 41:409
50. Watanabe H, Mukai T, Ishikawa K, Higashi K (2002) Scr Mater 46:851
51. Watanabe H, Mukai T, Ishikawa K, Higashi K (2003) Mater Sci Forum 419–422:557
52. Lapovok R, Cottam R, Thomson PF, Estrin Y (2005) J Mater Res 20:1375
53. Lapovok R, Thomson PF, Cottam R, Estrin Y (2005) Mater Sci Eng A 410–411:390
54. Figueiredo RB, Langdon TG (2006) Mater Sci Eng A 430:151
55. Miyahara Y, Matsubara K, Horita Z, Langdon TG (2005) Metall Mater Trans 36A:1705
56. Matsubara K, Miyahara Y, Horita Z, Langdon TG (2003) Acta Mater 51:3073
57. Furui M, Xu C, Aida T, Inoue M, Anada H, Langdon TG (2005) Mater Sci Eng A 410–411:439
58. Furui M, Kitamura H, Fukuta M, Anada H, Langdon TG (2007) Mater Sci Forum 539–543:2940
59. Furui M, Kitamura H, Anada H, Langdon TG (2007) Acta Mater 55:1083
60. Furukawa M, Ma Y, Horita Z, Nemoto M, Valiev RZ, Langdon TG (1998) Mater Sci Eng A 241:122
61. Lee S-M, Langdon TG (2001) Mater Sci Forum 357–359:321